



**HAL**  
open science

## Tissue Molecular Ion Imaging by Gold Cluster Ion Bombardment

David Touboul, Frédéric Halgand, Alain Brunelle, Reinhard Kersting, Elke Tallarek, Birgit Hagenhoff, Olivier Lapr evote

► **To cite this version:**

David Touboul, Frédéric Halgand, Alain Brunelle, Reinhard Kersting, Elke Tallarek, et al.. Tissue Molecular Ion Imaging by Gold Cluster Ion Bombardment. *Analytical Chemistry*, 2004, 76 (6), pp.1550-1559. 10.1021/ac035243z . hal-03976543

**HAL Id: hal-03976543**

**<https://hal.science/hal-03976543v1>**

Submitted on 13 Feb 2023

**HAL** is a multi-disciplinary open access archive for the deposit and dissemination of scientific research documents, whether they are published or not. The documents may come from teaching and research institutions in France or abroad, or from public or private research centers.

L'archive ouverte pluridisciplinaire **HAL**, est destin ee au d ep ot et  a la diffusion de documents scientifiques de niveau recherche, publi es ou non,  emanant des  tablissements d'enseignement et de recherche fran ais ou  trangers, des laboratoires publics ou priv es.

# Tissue Molecular Ion Imaging by Gold Cluster Ion Bombardment

*David Touboul<sup>1</sup>, Frédéric Halgand<sup>1</sup>, Alain Brunelle<sup>1</sup>, Reinhard Kersting<sup>2</sup>, Elke Tallarek<sup>2</sup>, Birgit  
Hagenhoff<sup>2</sup>, Olivier Laprèvote<sup>1</sup>*

<sup>1</sup> Institut de Chimie des Substances Naturelles, CNRS, Av. de la Terrasse, 91198 Gif-sur-Yvette Cedex,  
France

<sup>2</sup> Tascon GmbH, Mendelstraße 11, 48149 Münster, Germany

Authors for correspondence: [Alain.Brunelle@icsn.cnrs-gif.fr](mailto:Alain.Brunelle@icsn.cnrs-gif.fr), [Olivier.Laprevote@icsn.cnrs-gif.fr](mailto:Olivier.Laprevote@icsn.cnrs-gif.fr)

The use of gold cluster focused ion beams produced by a liquid metal ion gun in a TOF-SIMS mass spectrometer is shown to dramatically enhance secondary ion emission of phospholipids and peptides. The method has been successfully tested with cells grown onto plastic slips and with mouse brain slices, without any treatment of the samples. Very reliable time-of-flight mass spectra are acquired with a low primary ions dose of a few  $10^7$  ions, and high lateral resolution molecular ion images are obtained for heavy ions of great biological interest. This approach offers new opportunities in pharmacological and biological research fields by localizing compounds of interest such as drugs or metabolites in tissues.

Mass spectrometry offers, among other methods of spectroscopy, the almost unique possibility of detecting simultaneously a large number of molecular ions in a mixture. In biology, ion microprobes have successfully been used to localize chemical or biological compounds of interest.<sup>1</sup> Benninghoven was the first to demonstrate that molecular ions, as well as elemental ions, could be localized using Secondary Ion Mass Spectrometry (SIMS).<sup>2</sup> The state of the art in this field has very recently been reviewed by Belu *et al.*<sup>3</sup> Chait and Standing were the first to publish that it was possible to achieve significant improvements in both mass resolution and transmission efficiency using a time-of-flight (TOF) analyser for SIMS analysis of biological compounds.<sup>4</sup>

For surface analysis of biological samples or other molecular samples with a good lateral resolution (*i.e.* at the micrometer scale or less) the main problem lies in the poor desorption efficiency of the primary ions generally used. Ga<sup>+</sup> or In<sup>+</sup> liquid metal ion guns (LMIGs) provide excellent lateral resolutions of a few tens of nanometers,<sup>5,6,7</sup> but the images obtained from tissue samples are generally limited to ions like phosphatidylcholine head group of the membrane lipids at  $m/z$  184.<sup>8</sup> The contrast of the images is low although it is obtained with high primary ion doses, close to the static SIMS limit (commonly  $10^{13}$  ions.cm<sup>-2</sup>). The high impact energy (25 keV) of the Ga<sup>+</sup> ions, which is necessary to get sufficient secondary ion emission (SIE), induces the penetration of the projectiles for more than 40 nm depth (calculated from SRIM 2000 code tables<sup>9</sup>). Consequently, only a small part of the energy is deposited in the first layers close to the surface where it is known that the SIE processes take place (70% of the SIE comes from the first 5 nm on the surface).<sup>10</sup>

A real breakthrough in the ion imaging field was the introduction of Matrix - Assisted Laser Desorption Ionization (MALDI) which has shown its ability to obtain intact ions from large biomolecules of thousands of Daltons.<sup>11</sup> Caprioli and co-workers,<sup>12,13</sup> now followed by another group,<sup>14</sup> have taken advantage of the unique capabilities of this soft desorption method to obtain the first images of biological tissues with, in particular, the localization of biomacromolecules over the investigated surface. In typical MALDI - TOF imaging experiments, the laser spot diameter is ~30-50  $\mu$ m. The matrix must be applied in solution as a drop or spray, which can result in perturbing the distribution of

substances on the dried down tissue sample. The lateral resolution of MALDI - TOF imaging experiments is consequently limited to  $\sim 50 \mu\text{m}$ , which is not precise enough for many biological applications.

In SIMS, the use of polyatomic projectiles, instead of atomic ones, can strongly enhance the SIE yields, as was first observed in the pioneering experiments of Andersen and Bay.<sup>15</sup> These authors demonstrated that the sputtering yield (neutrals) induced by a diatomic projectile was higher than twice that induced by the atomic projectile at the same velocity. Cluster and molecular ions are a unique way to bombard simultaneously with several atoms a very small surface of a few ångströms square, increasing the energy density deposited close to the surface. The effects of polyatomic projectiles, both in the keV and in the MeV impact energy ranges have been reviewed by Le Beyec.<sup>16</sup> Fundamental studies have been carried out by Le Beyec and co-workers in the keV impact energy range, mainly using gold cluster beams from a LMIG. Large non linear enhancements of SIE were observed for organic and inorganic secondary ions.<sup>17,18,19</sup>

Over the past decade, a great interest has developed in the use of these new polyatomic projectiles to enhance the sensitivity of TOF-SIMS. It has been shown that the increase in sensitivity can be achieved without a concomitant increase in the extent of surface damage. Different polyatomic projectiles have been tested, such as  $\text{SF}_6^-$ ,  $\text{SF}_5^+$ ,<sup>20,21,22,23</sup> or glycerol clusters.<sup>24</sup> Fullerene ion sources seem to be very promising.<sup>25,26</sup> The higher efficiency of  $\text{C}_{60}^+$  ion beams, compared to  $\text{Au}_3^+$  or  $\text{Au}_4^+$  ion beams, was already demonstrated in 1994 by Boussofiane-Baudin *et al.*<sup>27</sup> All of these primary ion beam sources suffered from difficulties in achieving sufficient beam intensity when the beam was focused below  $1 \mu\text{m}$ , and are not presently suitable for biological imaging applications.

A gold LMIG can produce  $\text{Au}_n^+$  gold clusters with n being larger than 7 depending on the operating conditions. The lifetime of this kind of ion source can now be longer than one thousand of  $\mu\text{A}\cdot\text{hours}$  by using appropriate alloys of gold with silicon<sup>28</sup> or with germanium.<sup>29</sup> The very high brightness of these sources, combined with reasonable intensities, make them ideally suited for molecular ion imaging.<sup>30,31</sup> In particular,  $\text{Au}_3^+$  ion beams seem to be a good compromise between sensitivity enhancements, primary

ion intensity, pulse duration and lateral resolution. Heavier gold clusters containing more than 3 atoms might be more efficient but the ion beam currents are too low for imaging experiments within acceptable measurement time.

For all the reasons described above, we used gold cluster ion sources to desorb, with a very high lateral resolution ( $< 1 \mu\text{m}$ ) and a very high sensitivity, intact molecular ions of biological interest from test samples and from thin animal tissue samples. Our objective was to analyse the tissue directly without any preliminary preparation such as a matrix deposition. The goal of this paper is to demonstrate the efficiency of this novel approach to model peptides in mixtures and to the image analysis of a mouse brain section. Finally a pixel size of 400 nm in a  $50 \times 50 \mu\text{m}^2$  area is shown.

## EXPERIMENTAL SECTION

**Mass Spectrometry and Imaging MS.** All the experiments described in the present paper have been performed using a standard commercial TOF-SIMS IV (ION-TOF GmbH, Mendelstraße 11, 48149 Münster, Germany)<sup>32</sup> reflectron type time-of-flight mass spectrometer located in Tascon GmbH company (Münster, Germany). The primary ion source is a gold LMIG which delivers  $\text{Au}_n^+$  gold cluster ions, with  $n = 1-7$  ( we used  $n = 1$  and 3). The effective ion flight path is about 2 m, the reflectron is a single stage model (first order compensation). The secondary ions are accelerated to a kinetic energy of 2 keV and are post-accelerated to an energy of 10 keV before hitting a hybrid detector made of a single microchannel plate followed by a scintillator and a photomultiplier. A three lens ion column focuses the ion beam on the target plane to a spot having a typical size of 400-500 nm. The angle of incidence is  $45^\circ$ . A double blanking plate system ensures the primary ion mass selection with repetition rates up to 50 kHz. The primary ion current, which is measured using a Faraday cup located on the grounded sample holder, is 1 pA for  $\text{Au}_1^+$  and 0.05 pA for  $\text{Au}_3^+$  at 10 kHz. The pulse durations are 0.7 ns for  $\text{Au}_1^+$  and 1.2 ns for  $\text{Au}_3^+$ , ensuring sufficiently short pulses for time-of-flight analysis with a mass resolution exceeding  $M/\Delta M = 1.1 \cdot 10^4$  (FWHM) at  $m/z$  722.6. Time-of-flight mass spectra are recorded using a 512

multi stops time-to-digital converter having a minimum bin size of 50 ps. The mass calibration of the spectra was always internal, using  $H^+$ ,  $C^+$ ,  $CH^+$ ,  $CH_2^+$  and  $C_3H_2^+$  ion peaks in positive ion mode and  $C^-$ ,  $CH^-$ ,  $CH_2^-$ ,  $C_2^-$ ,  $C_3^-$ ,  $C_4^-$  and  $C_4H^-$  ion peaks in negative ion mode. Mass accuracies were always better than a few ppm.

The analyzed surface can be checked at any time by the operator with the help of a video camera. A low energy electron flood gun can be activated, between two pulses of the primary ion beam, when necessary to neutralize the surface of insulating samples.

For spectroscopy measurements, the irradiation time was always 100 s whatever the primary ion, over an irradiated area of  $200 \times 200 \mu m^2$ . The total primary ion doses are  $1.3 \cdot 10^9$  ions ( $3.25 \cdot 10^{12}$  ions. $cm^{-2}$ ) and  $3.1 \cdot 10^7$  ions ( $7.75 \cdot 10^{10}$  ions/ $cm^2$ ) for  $Au_1^+$  and  $Au_3^+$ , respectively. These ion doses are far below the static SIMS limit.

The typical acquisition time for imaging experiments was in the order of 1 hour. Principally, two modes of image acquisition can be selected:

i - Images with fields of view below  $500 \times 500 \mu m^2$  are performed without stage movement just by rastering the primary ion beam. There are several ion gun modes available to find the best compromise between primary ion current (measurement time), pulse length (mass resolution) and focus (lateral resolution). In total, the focus can vary between some  $\mu m$  and 100 nm and the pixel size can be selected by the operator between  $64 \times 64$  to  $1024 \times 1024$ .

ii - Large area analysis ( $500 \times 500 \mu m^2$  to  $9 \times 9 cm^2$ ) can be performed using the so called stage scan. In this mode the sample is continuously moved by the stage. The user can define the pixel size by selecting the number of pixels along the scanned area. In order to scan the whole surface area the primary ion beam is rastering over the area of a such defined individual pixel. For example, using  $128 \times 128$  pixels on an area of  $8 \times 8 mm^2$  results in a pixel size of  $62.5 \times 62.5 \mu m^2$ .

**Sample Preparation.** A synthetic phospholipid (PLP), 1-octadecanoyl,2-[cis-9,12]-octadecadienoyl-glycero-3-phosphocholine, (MW 786.60 Da, stock solution concentration of  $100 pmol \cdot \mu L^{-1}$ ) was

purchased from Sigma-Aldrich (BP 701 F-38297 St Quentin Fallavier, France). Three microliters of final solutions, diluted in a solution of nitrocellulose in acetone ( $20 \text{ mg}\cdot\text{mL}^{-1}$ ) and corresponding to sample concentrations of 10, 1 and  $0.1 \text{ pmol}\cdot\mu\text{L}^{-1}$  were deposited onto metallic plates. The peptide mixture named Pepmix4 was purchased from LaserBio Labs (1300 Route des Crêtes, F-06905 Sophia-Antipolis, France). This mixture is composed of the following peptides, for which the monoisotopic molecular weights are given:

- i- Bradykinin 1-5, RPPGF (amino-acid single letter code), MW 572.31 Da,
- ii- Angiotensin II, DRVYIHPF, MW 1045.53 Da,
- iii- Neurotensin, ELYENKPRRPYIL, MW 1671.91 Da,
- iv- ACTH 18-39 fragment, RPKVYPNGAEDESAEAFPLEF, MW 2464.19 Da,
- v- Bovine Insulin B chain, FVNQHLCGSHLVEALYLVCGERGFFYTPKT, MW 3493.64 Da.

Two microliters of the peptides mixture in  $\text{H}_2\text{O}/\text{TFA}$  (0.1%) diluted in a solution of  $20 \text{ mg}\cdot\text{mL}^{-1}$  of nitrocellulose in acetone and giving final concentrations of 2.0, 1.2, 0.8, 1.0 and  $5.0 \text{ pmol}\cdot\mu\text{L}^{-1}$  for the Bradykinin, Angiotensin II, Neurotensin, ACTH and Bovine Insulin B chain, respectively, were deposited onto metallic plates. Dilutions by factors 10 and 100 have also been made. The hydrophobic peptide E1-Nter was provided by courtesy from Dr. F. Penin (IBCP, Lyon France). The amino-acid sequence of this peptide is GAHWGVLAGIAYFSMVGWAK-NH<sub>2</sub>. Its monoisotopic molecular weight is 2233.13 Da and it has a GRAVY hydrophobicity index value of 0.595. Two microliters of final solutions, diluted in a solution of  $20 \text{ mg}\cdot\text{mL}^{-1}$  of nitrocellulose in acetone and having concentrations of 900 and  $90 \text{ fmol}\cdot\mu\text{L}^{-1}$  were deposited onto metallic plates.

Laminated metallic plates were purchased from Goodfellow (Ermine Business Park, Huntingdon PE29 6WR, England). The purity of the gold and copper plates is 99.99%, and the composition of the stainless steel (15-7PH) is Fe 75%, Cr 15%, Ni 7%, Mo 2.25% (weight %).

The mouse muscular cells were obtained from S. De La Porte (Laboratoire de Neurobiologie Cellulaire et Moléculaire, Gif-sur-Yvette, France). Cells were grown in a nutritive medium (DMEM) onto plastic cover slips (diameter 25 mm, Thermanox<sup>®</sup>, Nalge Nunc Intl, 75 Panorama Creek Drive,



Rochester, NY 14625. U.S.A.). The plastic slips were rinsed two times with a phosphate buffer saline solution (PBS) and with 1 mL of milliQ® water, dried and kept cold at -24°C.

The mouse brain was cut at a temperature of -18°C in a cryostat (model MGW Lauda 1720, Leica Microsystems SA, 86 Avenue du 18 Juin 1940, F-92563 Rueil-Malmaison, France). The tissue slices, which have a thickness of 15 µm, were immediately deposited onto the stainless steel or gold plate and kept at -80°C. Just before analysis the plates and slices were warmed to room temperature and dried under a pressure of a few hPa for ~1 h.

## RESULTS AND DISCUSSION

**Synthetic phospholipid.** Table 1 shows the SIE yields at  $m/z$  786.60 and  $m/z$  184 (molecular ion and phosphatidylcholine head group ion) on different metallic surfaces, with or without nitrocellulose, with  $Au_1^+$  and  $Au_3^+$  as primary ions. The SIE yields are calculated as the area of the peak of interest (number of detected ions) divided by the number of primary ions having impinged the surface during the acquisition of the spectrum. It is clear that the  $Au_3^+$  clusters, used as primary ions, induce SIE yields about ten times higher than those induced by  $Au_1^+$  ions. The observed enhancements confirm the previous results obtained elsewhere on smaller size molecules.<sup>18,19</sup> It must be noted that in these references the SIE yields were compared at the same impact velocity for different sizes of cluster projectiles. In the present standard analytical conditions, polyatomic projectiles are compared to atomic ones at the same total impact energy (25 keV), *i.e.* at different velocities.

The addition of nitrocellulose enhances the SIE yields. This enhancement is so high that the ion at  $m/z$  786.60 is observed only with nitrocellulose. This effect of nitrocellulose was reported previously in PDMS (Plasma Desorption Mass Spectrometry) by Jonsson *et al* but also in SIMS.<sup>33,34,35</sup> The best metallic plate is stainless steel, compared to gold or copper which do not allow a good desorption of the synthetic phospholipid ions. It is here surprising to note that although the deposited sample was rather thick (“dried droplet”), the composition of the metallic substrate still has an important influence on the SIE yields. The wetting properties or the surface quality of the metal, with regard to the solutions used,

can lead to more or less homogeneous samples that strongly influence the SIE yield values. However, the use of different plates shows different enhancement factors between  $\text{Au}_1^+$  and  $\text{Au}_3^+$ . It seems that the use of both a gold cluster ion source and nitrocellulose promotes the molecular ion formation rather than ion fragmentation. In addition to the molecular ion at  $m/z$  786.6 and when the sample is mixed with nitrocellulose and deposited on stainless steel (Figure 1), two diagnostic sodium cationized ions of the synthetic phospholipid at  $m/z$  808.6 ( $[\text{M}+\text{Na}]^+$ ) and  $m/z$  147 (sodium cationized cyclophosphonate) and non-covalent dimer ions of phospholipid at  $m/z$  1572.2 ( $[\text{2M}+\text{H}]^+$ ) and at  $m/z$  1594.2 ( $[\text{2M}+\text{Na}]^+$ ) were observed.<sup>36</sup> The ion at  $m/z$  184 (corresponding to the phosphatidylcholine head group) was observed in all cases whatever the preparation method and the metallic plate used.

Dilution tests have been done to evaluate the detection limit. Our results show that the minimal detectable concentration is about 1  $\mu\text{M}$ , when the synthetic phospholipid is mixed with nitrocellulose on stainless steel, which is rather comparable to MALDI-TOF detection limit.<sup>37</sup> Considering both that the irradiated surface is only  $200 \times 200 \mu\text{m}^2$  and that the deposited droplet is spread out on a 1.5 mm diameter, the quantity of phospholipid really consumed for the spectrum acquisition is 68 fmol.

**Peptides.** We have analyzed a commercial peptide mixture (Pepmix4), diluted with the previous nitrocellulose solution (see experimental) and deposited on a stainless steel plate. The measured SIE yields are presented in Table 2 and the corresponding mass spectra are shown in Figure 2. The higher desorption efficiency of  $\text{Au}_3^+$  cluster ions, compared to  $\text{Au}_1^+$ , is confirmed. The measured SIE yields decrease with increasing peptide molecular weight. This can be due to a lower desorption yield, or to the increase of metastability for high weight molecules, or to the decrease of the detection efficiency with lowering secondary ion velocity, particularly since a post-acceleration of only 10 kV was used.<sup>38,39,40</sup> Nevertheless, the characteristic ion of the ACTH peptide at  $m/z$  2465.19 has been detected with  $\text{Au}_3^+$  cluster ions, which is presently our upper mass limit. Considering the irradiated surface, the spreading of the droplet and the sample concentration, the real peptide consumption is about 45 fmol. A 20 kV

post-acceleration of the secondary ions should significantly improve the detection efficiency for larger mass compounds, such as Insulin B chain.

Afterwards, we have analyzed an hydrophobic peptide called E1-Nter for which characteristic ions are observed (Figure 3) at  $m/z$  2234.1 ( $[M+H]^+$ ) and  $m/z$  2256.1 ( $[M+Na]^+$ ). The detection limit has been evaluated at about 1  $\mu$ M. This experiment shows that it is possible to desorb hydrophobic peptides which are difficult to detect by other ionization methods, and which often require the use of special ionization methods like Atmospheric Pressure Photoionization.<sup>41</sup>

**Cells.** Mouse muscular cells have been directly analyzed on the plastic thin slips after one phosphate buffer and two water washes. A spectrum corresponding to the mass range of the phospholipid ions is shown in Figure 4. The SIE yield for  $m/z$  782.60 desorbed by  $Au_3^+$  cluster ions is about  $5 \cdot 10^{-6}$  and nitrocellulose is not essential to record good signals as shown in this figure. For this experiment, no MALDI matrix is necessary. The so-called “Matrix Enhanced SIMS” (ME-SIMS), although it could enhance the SIE yields, is here not essential.<sup>42,43</sup> Biological environment seems to play the role of “natural matrix”, although one must be careful with such statements. We were working with dried down cells or tissue cross-sections, which cannot really be called a “biological environment”. Obviously, as the samples were carefully prepared, then the spatial organization of the sample was retained and the spatial distribution and relative intensities of the observed masses could be related back to the biological environment. This remark holds also for the following tissue imaging section.

In the case of the synthetic phospholipid, careful scrutiny of the spectra indicates an intensity ratio  $I([M+H]^+)/I([M+Na]^+)$  close to 1.75 for an intensity ratio  $I(m/z 184)/I(m/z 147)$  close to 4.07. The  $m/z$  184 ion originates from protonated molecules whereas the fragment ion at  $m/z$  147 arises from the dissociation of the sodium cationized molecule. Thus for cell cultures, the value of 1.89 of the  $I(m/z 184)/I(m/z 147)$  ratio suggests that the major form of phospholipid ions is sodium cationized. This can be explained by the use of a phosphate buffer wash and the presence of sodium in cellular environment.

**Tissue slices: Spectroscopy.** Encouraged by our results on cellular cultures, we decided to study mouse brain slices, directly deposited on a stainless steel plate without nitrocellulose or any other matrix. Such experiments have been already done with  $\text{Ga}^+$  or  $\text{In}^+$  as primary ions.<sup>3,44</sup> Unfortunately, the very low SIE yields with those ion sources enable only analysis over a low mass range, typically limited up to  $m/z \sim 300$ . In addition, the primary ion doses were close to the static SIMS limit, leading to significant damage on the biological tissue surface. The intense SIE under  $\text{Au}_3^+$  cluster ion irradiation consequently enlarges the observable mass range up to  $m/z = 900$  Da (Figures 5 and 6). Many ion structures, different from phospholipid ones, have been identified by exact mass measurements (<5 ppm) and by comparison between positive and negative ionisation modes.

The spectra of Figure 5 and Figure 6 can be described as follows:

- i- Low mass ion peaks ( $\text{Na}^+$ ,  $\text{K}^+$ ... /  $\text{Cl}^-$ ,  $\text{Br}^-$ ...) are very intense.
- ii- The characteristic ions of phospholipids such as  $m/z$  147 or  $m/z$  184 are clearly identified. On the tissue slice, the ratio  $I(m/z\ 184)/I(m/z\ 147)$  is 10.47, indicating that the protonated form of phospholipids is dominating.
- iii- The positive ion spectrum shows 2 isotopic patterns at  $m/z$  369 and  $m/z$  385 respectively, and the negative ion spectrum, one profile at  $m/z$  385. We can conclude that cholesterol ( $m/z$  385 for  $[\text{M}-\text{H}]^+$  and  $m/z$  369 for  $[\text{M}-\text{H}_2\text{O}+\text{H}]^+$ ) is present in mouse brain slices. In the negative ion mode, the peak at  $m/z$  385 corresponds to the deprotonated molecule  $[\text{M}-\text{H}]^-$ .
- iv- In the mass range  $470\ \text{Da} \leq m/z \leq 530\ \text{Da}$ , in the positive ion mode, many ions are present and could correspond to diglycerides coming from phospholipid or triglyceride fragmentations. At this stage, we are not able to conclude on the exact origin of those ions.
- v- Many other peaks in the negative ion mode have not yet been identified and further experiments are needed.

**Tissue slices: Yields, Disappearance Cross Section and Efficiencies.** In order to compare efficiency of the ion generation process under  $Au_1^+$  and  $Au_3^+$  bombardment the following values were determined directly from the tissue slices: SIE yield  $Y$  (already defined above), disappearance cross section  $\sigma$  and secondary ion generation efficiency  $E$ . The values are defined as follows:

i - Disappearance cross section  $\sigma$ :  $N(t) = N(t=0).exp(-\sigma I/Ae)$

with:  $N(t)$ : number of detected particles at time  $t$ ;  $N(t=0)$  number of detected particles at time 0;  $I$ : primary ion current;  $A$ : bombarded area;  $e$ : elemental charge; for samples of multilayer thickness contributions from deeper layers can influence  $\sigma$ , which is the mean area damaged by one primary ion and which is a parameter depending on the respective secondary ion species under consideration.

ii - Secondary ion generation efficiency  $E$ :  $E = Y/\sigma$ ;  $E$  is the number of detected secondary ions of a given species per damaged area.

The disappearance cross section for the  $(M-H)^+$  secondary ion of cholesterol was determined by bombarding an area of  $100 \times 100 \mu m^2$  and monitoring the secondary ion intensity as a function of time (decay curve). From the slope of the decay curve  $\ln(I)$  versus time,  $\sigma$  can be calculated. For the yield determination spectra were taken for 15 s only. Peak integral values were determined and yields were calculated by dividing the peak integral values by the primary ion dose. The corresponding efficiency  $E$  was determined by dividing the obtained yields by the corresponding disappearance cross sections. Data were taken for  $Au_1^+$  and  $Au_3^+$  bombardment from 2 freshly selected positions each. The results are summarised in Table 3 showing the average values over the 2 positions.

As one can see the yield increases by a factor of 30 when switching from  $Au_1^+$  to  $Au_3^+$  whereas the disappearance cross section only rises by a factor of 1.9 resulting in an efficiency enhancement by a factor of 19. Therefore,  $Au_3^+$  bombardment is superior to  $Au_1^+$  bombardment when aiming at low detection limits. A tissue slice is obviously not a homogeneous surface and is consequently not best suited to measure precisely the above values, which can significantly change from one irradiated area to

another. Nevertheless, the enhancement of  $E$  is certainly significant and can be considered for the following section.

**Tissue slices: Imaging.** The feasibility of acquiring a spectrum on a tissue slice with an excellent sensitivity, prompted us to acquire ion images of a mouse brain slice. Different lateral resolutions with  $\text{Au}_3^+$  clusters have been tested to localize several known biological compounds.

The area of the square circumscribed by the slice is  $8 \times 8 \text{ mm}^2$ . The corresponding image ( $128 \times 128$  pixels) is achieved in 1h30 with a spatial resolution of  $62.5 \text{ }\mu\text{m}$ , 256 shots per pixel and  $600 \text{ Au}_3^+$  ions per shot (*i.e.*  $1.54 \cdot 10^5$  projectiles per pixel). Figure 7a displays images corresponding to the iron ion signal, outside of the slice, to the sum of cholesterol ions and to the sum of phospholipid ions. These 3 images are exactly complementary one to each other which proves that avoiding treatment of the tissue slice is of crucial importance to prevent ion delocalization. This spatial resolution makes it possible to obtain a global molecular image of a biological tissue slice. The localization of phospholipid ions can be compared to the ion image by Todd *et al* with a  $\text{Ga}^+$  primary ion source.<sup>44</sup> Different zones are precisely identified with an anatomic atlas<sup>45</sup> as the *corpus callosum*, the *anterior commissure*, the *nucleus triangularis septi* and the *caudate putamen* where cholesterol signals are very high. The presence of cholesterol can be linked to its role in membrane fluidity modulations<sup>46</sup> and in membrane receptor activity (for example : ocytocine receptor<sup>47</sup>). Moreover the detection of cholesterol in the *corpus callosum*, which transfers information from one hemisphere to the other, can be related to a regulation of peptides and hormones transport.<sup>48</sup>

In order to compare the efficiencies of  $\text{Au}_1^+$  and  $\text{Au}_3^+$  projectiles, two images were acquired with the same primary ion dose of  $1.5 \cdot 10^8$  ions. The size of these images was  $500 \times 500 \text{ }\mu\text{m}^2$  with a pixel size of  $1.96 \text{ }\mu\text{m}$  ( $256 \times 256$  pixels). Both irradiations were made very close one to each other and at the edge of the *corpus callosum*. Images corresponding to the cholesterol and to the phospholipid ions are shown in Figure 7b. With  $\text{Au}_3^+$  used as a primary ion, the inner and the outer of the *corpus callosum* are clearly

distinguished with the spatial distribution of these two secondary ions, while barely distinguished when using the same dose of  $\text{Au}_1^+$  primary ions. It is clear that at equal irradiation doses,  $\text{Au}_3^+$  projectiles give ion images with a much better quality than  $\text{Au}_1^+$  ions, for which the same secondary ion intensities could be obtained only with a higher dose, *i.e.* with a higher surface damage.

Finally, an image of an inner part of *corpus callosum* was obtained, corresponding to a surface of  $54.7 \times 54.7 \mu\text{m}^2$  and with a lateral resolution of 427 nm (Figure 7c). Some unexplained micrometric substructures of the *corpus callosum* can be observed in that case.

This result demonstrates that it is possible to acquire images of biologically interesting ions on a tissue slice without any treatment, with lateral resolution decreasing to a few hundreds of nanometers and very low irradiation doses compared to the static SIMS limit.

## CONCLUSION

A new method of acquiring mass spectrometric images of heavy molecular ions shows promise for the detection of drugs and other small and intermediate organic molecules within biological samples. High sensitivity and high lateral resolution are now achieved with very low primary ion doses with gold cluster liquid metal ion guns and without any treatment or matrix deposition on the samples. Some improvements are expected with the development of new polyatomic primary ion beams like  $\text{C}_{60}^+$ . Increased post acceleration energy should also contribute to a better ion detection efficiency and thus increase the sensitivity in the high mass range, combined with a high lateral resolution compatible with imaging at the cellular level.

## ACKNOWLEDGMENTS

Sabine De La Porte, Vincent Voisin (Laboratoire de Neurobiologie Cellulaire et Moléculaire, Gif sur Yvette) and H el ene Piedno el (ICSN-CNRS Gif-sur-Yvette) are warmly thanked for their graciousness in

preparing and in taking care of the cells and tissue samples. Many thanks to Colin Helliwell (ION-TOF GmbH) for his assistance when reviewing the manuscript. D.T. is indebted to the Institut de Chimie des Substances Naturelles (CNRS) for a Ph.D. research fellowship.



Table 1: Secondary ion emission yields at  $m/z$  786.06 and  $m/z$  184 on different metallic surfaces, with or without nitrocellulose, with  $\text{Au}_1^+$  and  $\text{Au}_3^+$  as primary ions at an impact energy of 25 keV. Empty boxes mean that the secondary ion peak was not observed in the spectrum.

Preparation	Metallic plate	Ion $m/z$ 786.6			Ion $m/z$ 184		
		$\text{Au}_1^+$	$\text{Au}_3^+$	$\text{Au}_3^+/\text{Au}_1^+$	$\text{Au}_1^+$	$\text{Au}_3^+$	$\text{Au}_3^+/\text{Au}_1^+$
Pure	Stainless steel	-	-	-	$3.20 \cdot 10^{-05}$	$9.30 \cdot 10^{-04}$	29
Pure	Copper	-	-	-	$7.10 \cdot 10^{-05}$	$1.20 \cdot 10^{-03}$	16.9
Pure	Gold	-	-	-	$5.20 \cdot 10^{-05}$	$1.30 \cdot 10^{-03}$	25.0
on NC*	Stainless steel	$1.28 \cdot 10^{-06}$	$1.40 \cdot 10^{-05}$	10.9	$2.50 \cdot 10^{-05}$	$4.40 \cdot 10^{-04}$	17.6
mixed with NC*	Stainless steel	$1.68 \cdot 10^{-05}$	$1.19 \cdot 10^{-04}$	7.1	$1.34 \cdot 10^{-03}$	$8.38 \cdot 10^{-03}$	6.25
mixed with NC*	Copper	$2.58 \cdot 10^{-07}$	$1.14 \cdot 10^{-06}$	4.4	$1.69 \cdot 10^{-04}$	$1.30 \cdot 10^{-03}$	7.7
mixed with NC*	Gold	$1.32 \cdot 10^{-07}$	$1.10 \cdot 10^{-05}$	83.3	$8.82 \cdot 10^{-06}$	$6.79 \cdot 10^{-04}$	77.0

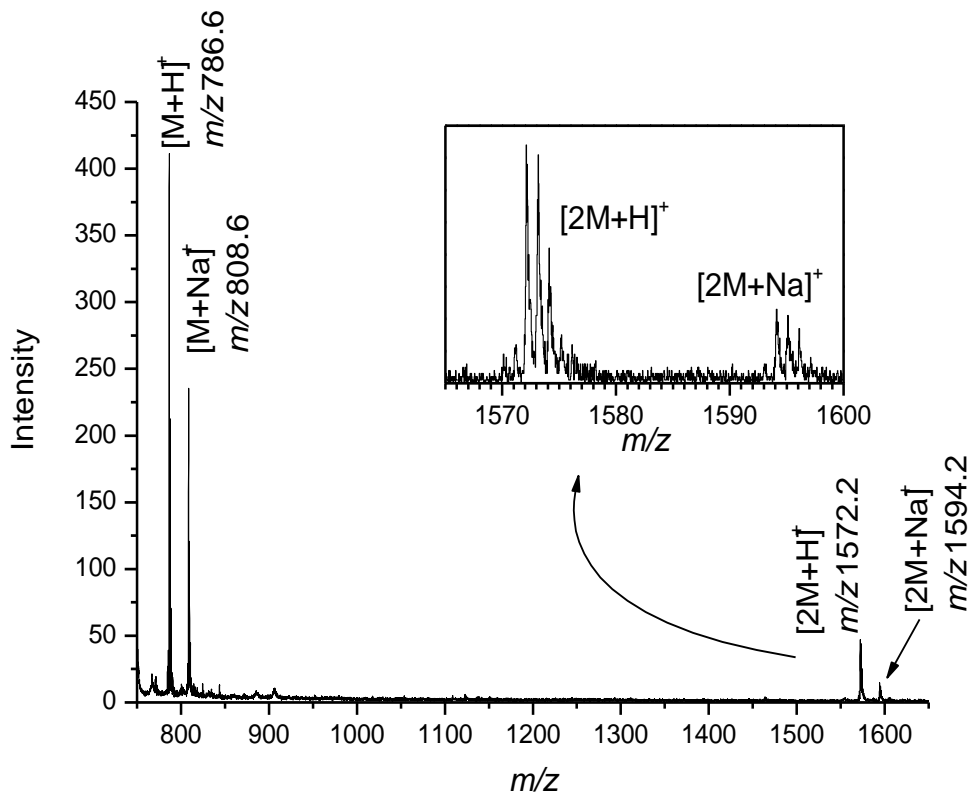
\*NC: nitrocellulose.

Table 2: Secondary ion emission yields for  $[M+H]^+$  ions of peptides, mixed with nitrocellulose, on stainless steel plate and with  $Au_1^+$  and  $Au_3^+$  as primary ions. Empty boxes mean that the secondary ion peak was not observed in the spectrum.

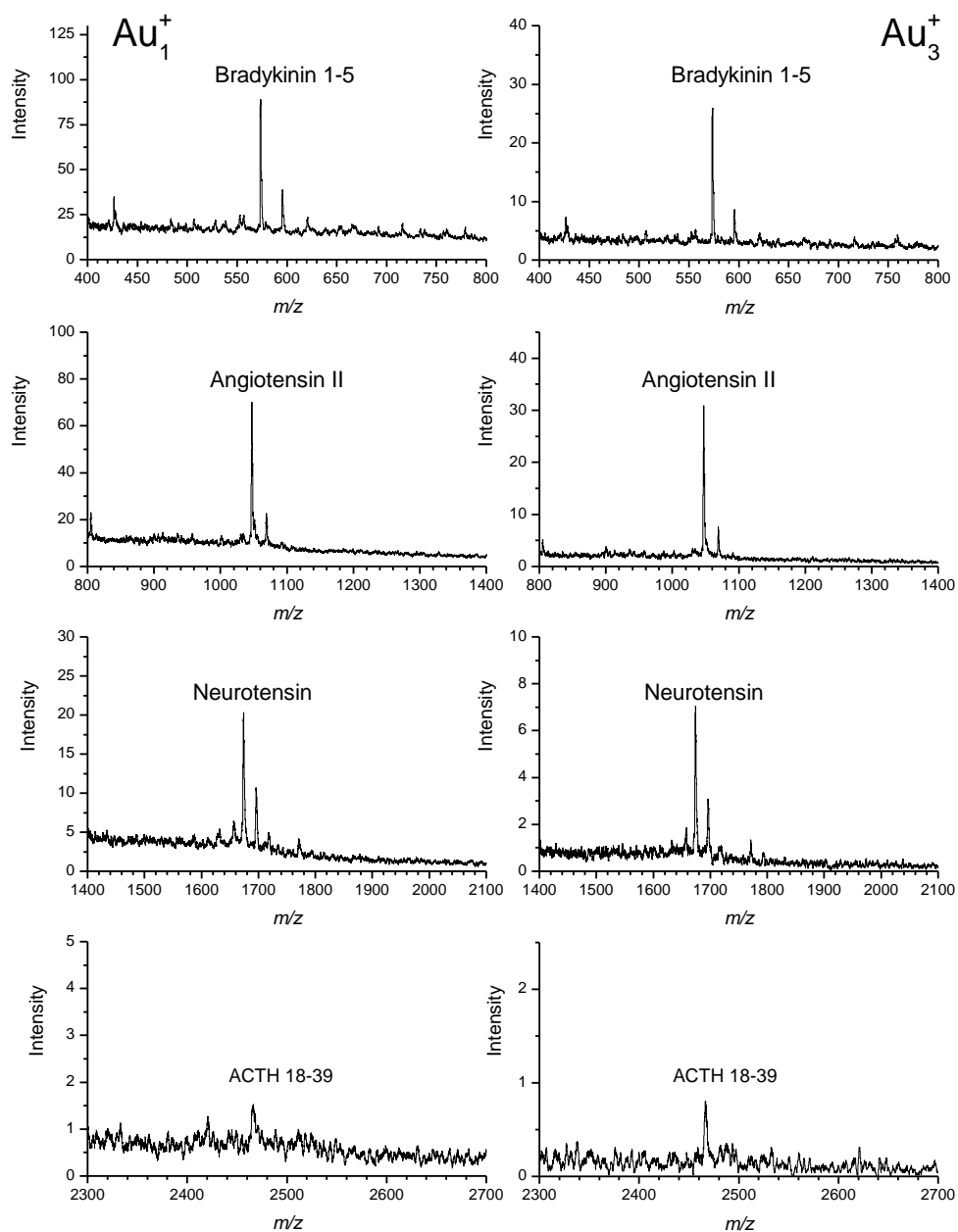
Secondary ion	$m/z$	Secondary ion yield		Relative yield
		$Au_1^+$	$Au_3^+$	$Au_3^+ / Au_1^+$
Bradykinin 1-5	573.32	$4.3 \cdot 10^{-6}$	$1.5 \cdot 10^{-5}$	3.5
Angiotensin II	1046.54	$2.5 \cdot 10^{-6}$	$1.3 \cdot 10^{-5}$	5.4
Neurotensin	1672.92	$5.9 \cdot 10^{-7}$	$2.4 \cdot 10^{-6}$	4.0
ACTH 18-39	2465.20	$4.3 \cdot 10^{-8}$	$2.1 \cdot 10^{-7}$	4.8
Insulin B chain	3494.65	-	-	-

Table 3: Secondary ion yields  $Y$ , disappearance cross sections  $\sigma$  and ion bombardment efficiencies  $E$  for  $\text{Au}_1^+$  and  $\text{Au}_3^+$  bombardment of cholesterol ( $[\text{M-H}]^+$ ;  $m/z$  385) in a brain section.

Primary Ion	$Y$	$\sigma$ (cm <sup>2</sup> )	$E$ (cm <sup>-2</sup> )
$\text{Au}_1^+$	$2.13 \cdot 10^{-5}$	$3.92 \cdot 10^{-13}$	$5.43 \cdot 10^{+7}$
$\text{Au}_3^+$	$6.60 \cdot 10^{-4}$	$6.36 \cdot 10^{-13}$	$1.04 \cdot 10^{+9}$



**Figure 1:** TOF-SIMS mass spectrum ( $\text{Au}_3^+$  cluster ion desorption) of a synthetic phospholipid at a concentration of  $100 \mu\text{M}$ , mixed with a solution of nitrocellulose ( $20 \text{ mg}\cdot\text{mL}^{-1}$  in acetone) and deposited on a stainless steel plate.



**Figure 2:** TOF-SIMS mass spectra of a commercial peptide mixture Pepmix4 (see text), mixed with a solution of nitrocellulose ( $20 \text{ mg}\cdot\text{mL}^{-1}$  in acetone), deposited on a stainless steel plate, with  $\text{Au}_1^+$  (left, dose  $9.83\cdot 10^8$  ions) or  $\text{Au}_3^+$  (right, dose  $8.26\cdot 10^7$  ions) as primary ions.

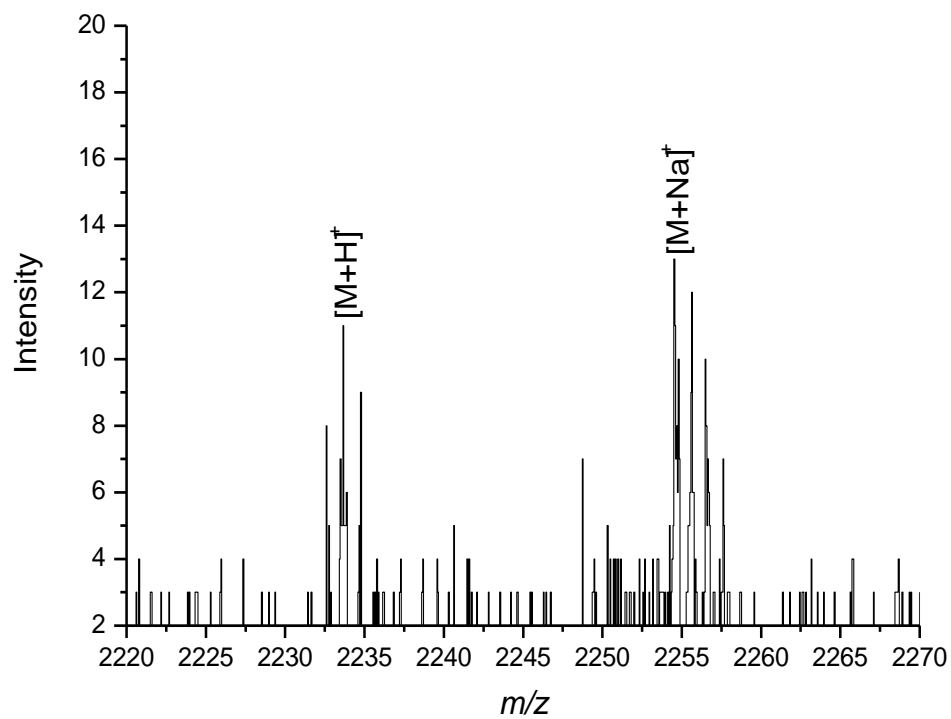


**Figure 3:** TOF-SIMS mass spectrum ( $\text{Au}_3^+$  cluster ion desorption) of a hydrophobic peptide E1-Nter at a concentration of  $9 \mu\text{M}$ , mixed with a solution of nitrocellulose ( $20 \text{ mg}\cdot\text{mL}^{-1}$  in acetone) and deposited on a stainless steel plate.

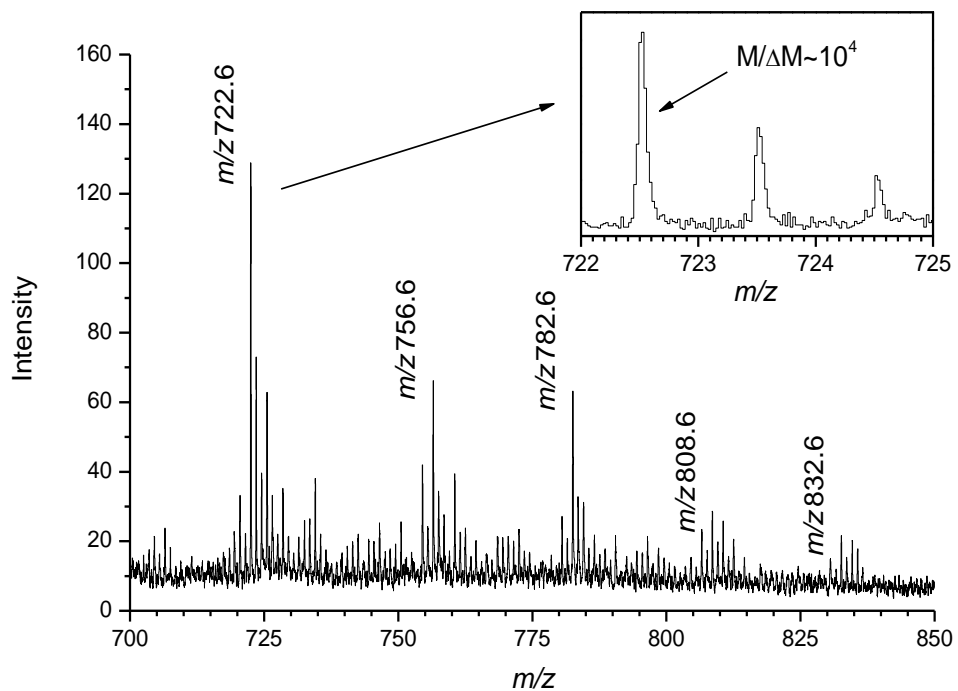


**Figure 4:** TOF-SIMS mass spectrum ( $\text{Au}_3^+$  cluster ion desorption) of a cellular culture without any matrix (data in the inset have been compressed for clarity of the figure).

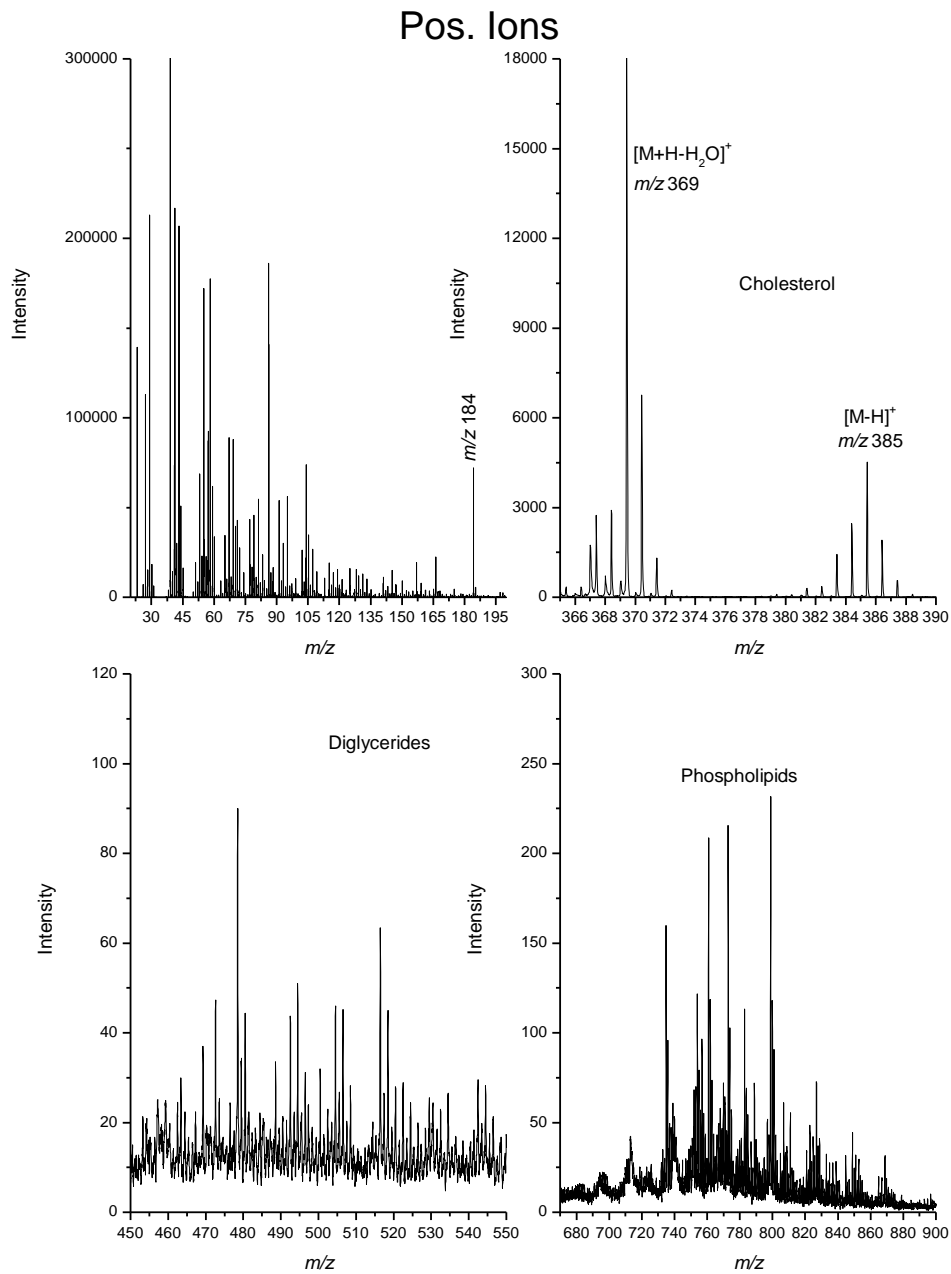


**Figure 5:** TOF-SIMS mass spectrum in positive ion mode ( $Au_3^+$  cluster ion desorption) of a mouse brain slice deposited on a stainless steel plate without treatment.



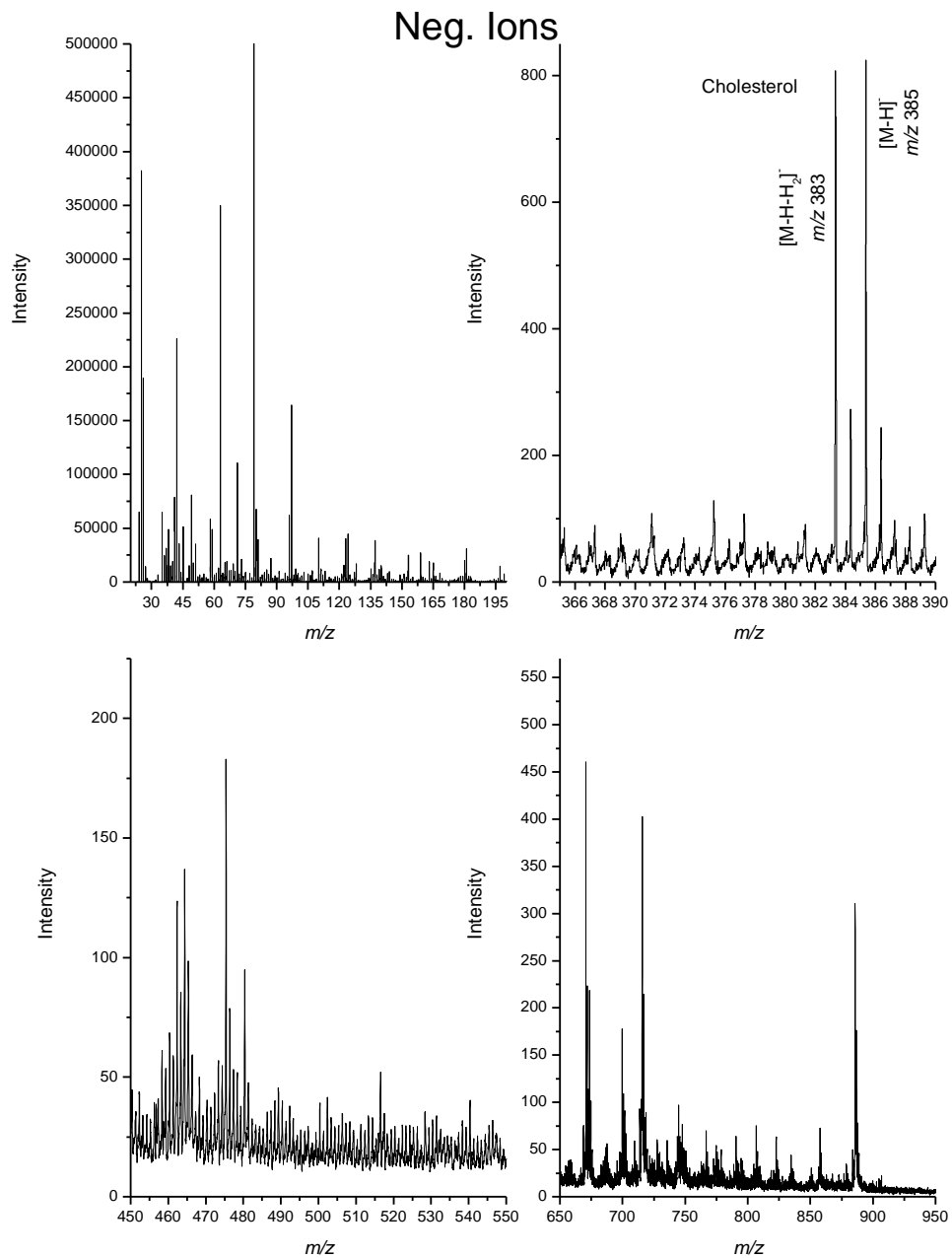


**Figure 6:** TOF-SIMS mass spectrum in negative ion mode ( $\text{Au}_3^+$  cluster ion desorption) of a mouse brain slice deposited on a stainless steel plate without treatment.

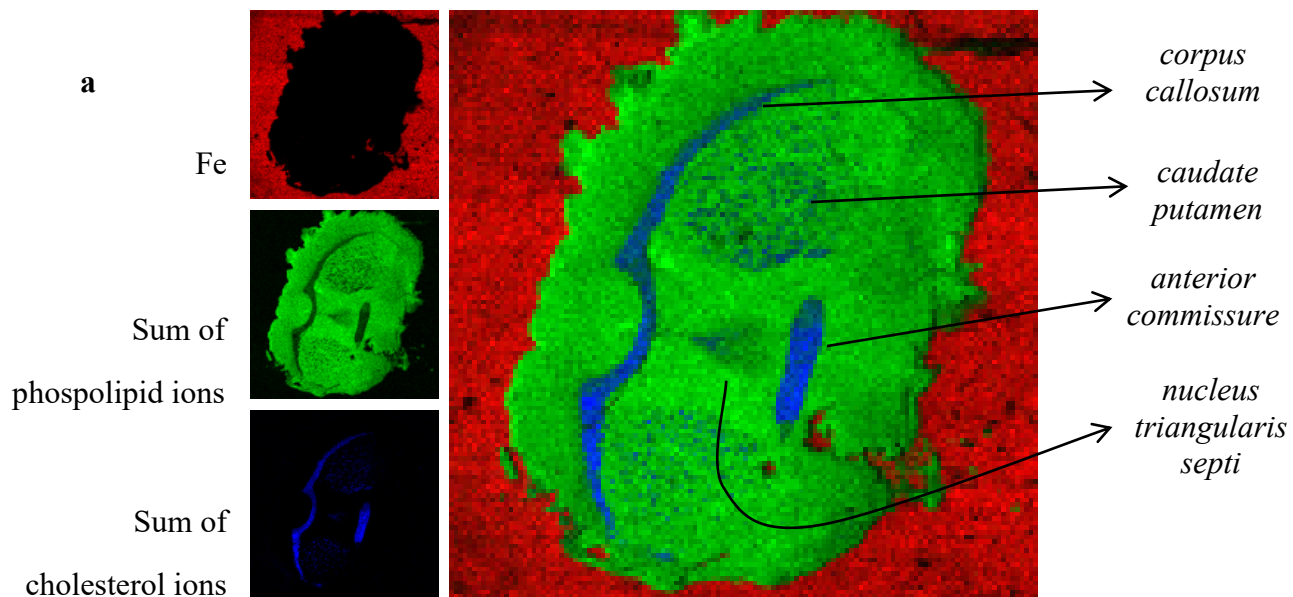


**Figure 7a:** Ion images of a mouse brain slice deposited on a stainless steel plate without treatment and for different biological molecules of interest. Field of view  $8 \times 8 \text{ mm}^2$ ; pixel size  $62.5 \text{ }\mu\text{m}$ ; individual images and overlay;  $\text{Au}_3^+$  projectiles.

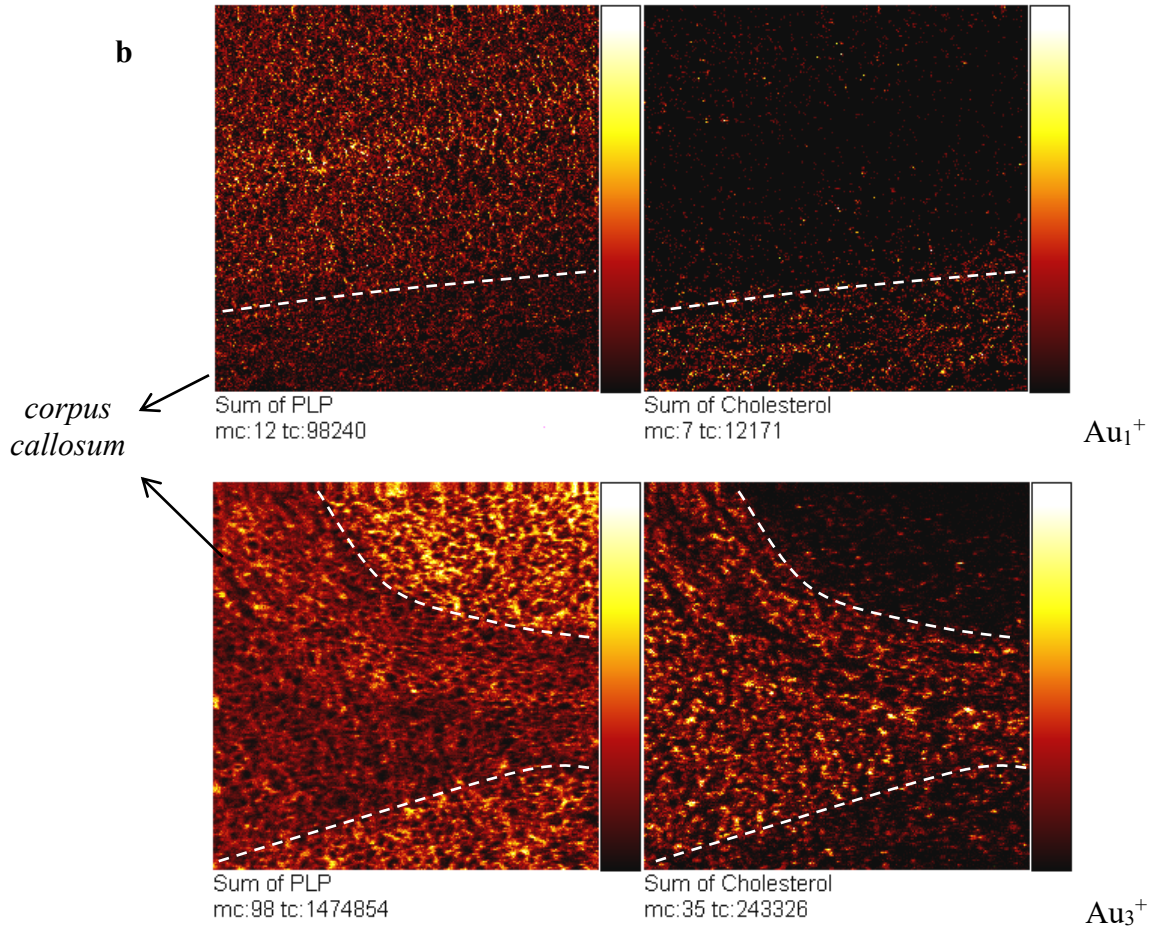


**Figure 7b:** Ion images taken at the edge of *corpus callosum* of a mouse brain slice deposited on a stainless steel plate without treatment and for different biological molecules of interest. Comparison between  $\text{Au}_1^+$  (top) and  $\text{Au}_3^+$  (bottom) projectiles; all data taken in two adjacent regions and at the same dose ( $1.5 \cdot 10^8$ ); field of view  $500 \times 500 \mu\text{m}^2$ ; pixel size  $1.95 \mu\text{m}$ .

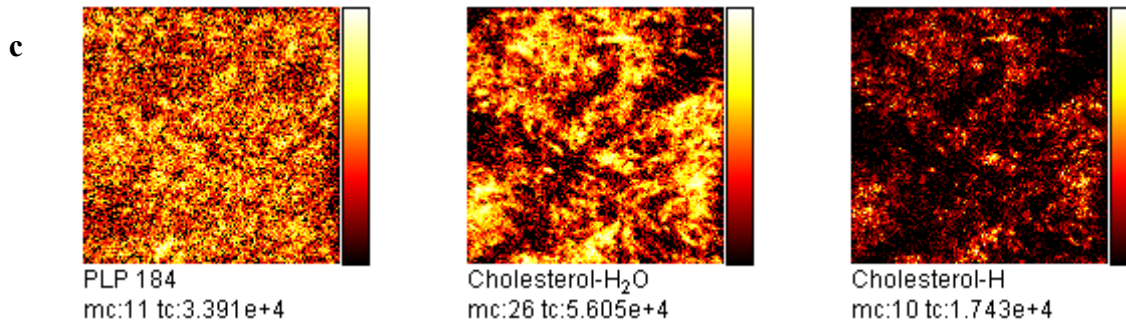


**Figure 7c:** Ion images of a mouse brain slice deposited on a stainless steel plate without treatment and for different biological molecules of interest. Field of view  $54.7 \times 54.7 \mu\text{m}^2$ ; pixel size 427 nm (inner part of *corpus callosum*);  $\text{Au}_3^+$  projectiles.

- (1) Castaing, R.; Slodzian, G. *J. Microsc.* **1962**, *1*, 395-410.
- (2) Benninghoven, A.; Loebach, E. *Rev. Sci. Instrum.* **1971**, *42*, 49-52.
- (3) Belu, A.M.; Graham, D.J.; Castner D.G. *Biomaterials* **2003**, *24*, 3635-3653.
- (4) Chait, B.T.; Standing K.G. *Int. J. Mass Spectrom. Ion Phys.* **1981**, *40*, 185-193.
- (5) Sudraud, P.; Van de Walle, J.; Colliex, C.; Castaing, R. *Surf. Sci.* **1978**, *70*, 392-402.
- (6) Levi-Setti, R.; Fox, T.R. *Nucl. Instrum. Methods* **1980**, *168*, 139-149.
- (7) Levi-Setti, R.; Hallégot, P.; Girod, C.; Chabala, J.M.; Li, J.; Sodonis, A.; Wolbach, W. *Surf. Sci.* **1991**, *246*, 94-106.
- (8) Pacholski, M.L.; Cannon, D.M.; Ewing, A.G.; Winograd, N. *Rapid Commun. Mass Spectrom.* **1998**, *12*, 1232-1235.
- (9) Ziegler, J.F.; Biersack, J.P.; Littmark, H. SRIM 2000.40, The Stopping and Ranges of Ions in Solids; Pergamon Press, New York, 1985.
- (10) Bolbach, G.; Viari, A.; Galera, R.; Brunot, A.; Blais, J.C. *Int. J. Mass Spectrom. Ion Processes* **1992**, *112*, 93-100.
- (11) Karas, M.; Bachmann, D.; Bahr, U.; Hillenkamp, F. *Int. J. Mass Spectrom. Ion Processes* **1987**, *78*, 53-68.
- (12) Caprioli, R.M.; Farmer, T.B.; Gile, J. *Anal. Chem.* **1997**, *69*, 4751-4760.
- (13) Stoeckli, M.; Chaurand, P.; Hallahan, D.E.; Caprioli, R.M. *Nat. Med.* **2001**, *7*, 493-496.
- (14) Stoeckli, M.; Staab, D.; Staufenbiel, M.; Wiederhold, K.H.; Signor, L. *Anal. Biochem.* **2002**, *311*, 33-39.

- (15) Andersen, H.H.; Bay, H.L. *J. Appl. Phys.* **1974**, *45*, 953-954.
- (16) Le Beyec, Y. *Int. J. Mass Spectrom. Ion Processes.* **1998**, *174*, 101-117.
- (17) Blain, M.G.; Della-Negra, S.; Joret, H.; Le Beyec, Y.; Schweikert, E.A. *Phys. Rev. Lett.* **1989**, **63**, 1625-1628.
- (18) Benguerba, M.; Brunelle, A.; Della-Negra, S.; Depauw, J.; Joret, H.; Le Beyec, Y.; Blain, M.G.; Schweikert, E.A.; Ben Assayag, G.; Sudraud, P. *Nucl. Instrum. Methods Phys. Res. B* **1991**, *62*, 8-22.
- (19) Brunelle, A.; Della-Negra, S.; Depauw, J.; Jacquet, D.; Le Beyec, Y.; Pautrat, M.; Baudin, K.; Andersen, H.H. *Phys. Rev. A* **2001**, *63*, 022902 1-10.
- (20) Appelhans, A.D.; Delmore, J.E. *Anal. Chem.* **1989**, *61*, 1087-1093.
- (21) Szymczak, W.; Wittmaack, K. *Nucl. Instrum. Methods. Phys. Res. B* **1994**, *88*, 149-153.
- (22) Gillen, G.; Roberson, S. *Rapid Commun. Mass Spectrom.* **1998**, *12*, 1303-1312.
- (23) Kötter, F.; Benninghoven, A. *Appl. Surf. Sci.* **1998**, *133*, 47-57.
- (24) Mahoney, J.F.; Cornett, D.S.; Lee, T.D. *Rapid Commun. Mass Spectrom.* **1994**, *8*, 403-406.
- (25) Weibel, D.; Wong, S.; Lockyer, N.; Blenkinsopp, P.; Hill, R.; Vickerman, J.C. *Anal. Chem.* **2003**, *75*, 1754-1764.
- (26) Postawa, Z.; Czerwinski, B.; Szewczyk, M.; Smiley, E.J.; Winograd, N.; Garrison, B.J. *Anal. Chem.* **2003**, *75*, 4402-4407.
- (27) Boussofiane-Baudin, K.; Brunelle, A.; Bolbach, G.; Della-Negra S.; Håkansson, P.; Le Beyec, Y. *Nucl. Instrum. Methods. Phys. Res. B* **1994**, *88*, 160-163.
- (28) Attal, P.; Della-Negra, S.; Gardès, D.; Larson, J.D.; Le Beyec, Y.; Vienet-Legué, R.; Waast, B. *Nucl. Instrum. Methods. Phys. Res. A* **1993**, *328*, 293-299.

- (29) Davies, N.; Weibel, D.E.; Blenkinsopp, P.; Lockyer, N.; Hill, R.; Vickerman, J.C. *Appl. Surf. Sci.* **2003**, *203-204*, 223-227.
- (30) Hagenhoff, B.; Kresting, R.; Rading, D.; Kayser, S.; Niehuis, E. In *Secondary Ion Mass Spectrometry, SIMS XII Proceedings*; Benninghoven, A., Bertrand, P., Migeon, H.-N., Werner, H.W., Eds.; Elsevier: Amsterdam, 2000; 833-836.
- (31) Kersting, R.; Pijpers, A.P.; Hagenhoff, B.; Verlaeck, R.; Stapel, D.; Benninghoven, A. In *Secondary Ion Mass Spectrometry, SIMS XII Proceedings*; Benninghoven, A., Bertrand, P., Migeon, H.-N., Werner, H.W., Eds.; Elsevier: Amsterdam, 2000; 825-828.
- (32) TOF-SIMS IV product description – Sept. 2002, ION-TOF GmbH, Mendelstr. 11, 48149 Muenster, Germany.
- (33) Jonsson, G.P.; Hedin, A.B.; Håkansson, P.L.; Sundqvist, B.U.R.; Såve, B.G.; Nielsen, P.F.; Roepstorff, P.; Johansson, K.E.; Kamensky, I.; Lindberg, M.S.L. *Anal. Chem.* **1986**, *58*, 1084-1087.
- (34) Lafortune, F.; Beavis, R.; Tang, X.; Standing, K.G.; Chait, B.T. *Rapid Commun. Mass Spectrom.* **1987**, *1*, 114-116.
- (35) Tonkinson, J.L.; Stillman, B.A. *Frontiers in Bioscience* **2002**, *7*, 1-12.
- (36) Griffiths, W.J. *Mass Spectrom. Rev.* **2003**, *22*, 81-152.
- (37) Andersen, J.S.; Svensson, B.; Roepstorff, P. *Nat. Biotechnol.* **1996**, *14*, 449-457.
- (38) Brunelle, A.; Chaurand, P.; Della-Negra, S.; Le Beyec, Y.; Parilis, E. *Rapid Commun. Mass Spectrom.* **1997**, *11*, 353-362.
- (39) Westmacott, G.; Ens, W.; Standing, K.G. *Nucl. Instrum. Methods Phys. Res. B* **1996**, *108*, 282-289.
- (40) Gilmore, I.S., Seah, M.P. *Int. J. Mass Spectrom.* **2000**, *202*, 217-229.

- (41) Delobel, A.; Halgand, F.; Laffranchise-Gosse, B.; Snijders, H.; Laprévotte, O. *Anal. Chem.* **2003**, *75*, 5961-5968.
- (42) Wu, K.J.; Odom, R.W. *Anal. Chem.* **1996**, *68*, 873-882.
- (43) Szymczak, W.; Wittmaack, K. *Rapid Commun. Mass Spectrom.* **2002**, *16*, 2025-2033.
- (44) Todd, P.J.; Schaaff, T.G.; Chaurand, P.; Caprioli, R.M. *J. Mass Spectrom.* **2001**, *36*, 355-369.
- (45) The rat brain in stereotaxic coordinates, 4<sup>th</sup> edition, G. Paxinos & Ch. Watson; Academic Press, London, 1998.
- (46) Wood, W.G.; Schroeder, F.; Avdulov, N.A.; Chochina, S.V.; Igbavboa, U. *Lipids* **1999**, *34*, 225-234.
- (47) Gimpl, G.; Burger, K.; Fahrenholz, F. *Biochemistry* **1997**, *36*, 10959-10974.
- (48) Geffen, G.M.; Jones, D.L.; Geffen, L.B. *Behav. Brain Res.* **1994**, *64*, 131-140.